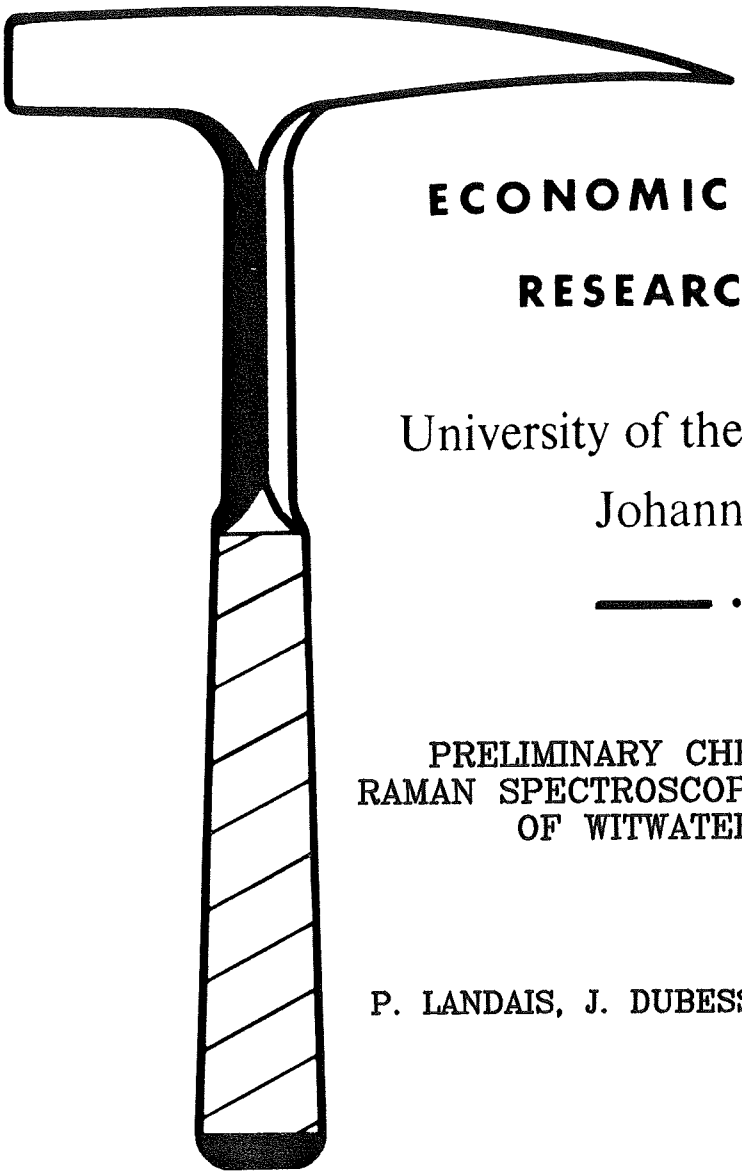

ECONOMIC GEOLOGY

RESEARCH UNIT

University of the Witwatersrand

Johannesburg

PRELIMINARY CHEMICAL ANALYSES AND RAMAN SPECTROSCOPY ON SELECTED SAMPLES OF WITWATERSRAND KEROGEN

P. LANDAIS, J. DUBESSY, L.J. ROBB AND C. NOUEL

INFORMATION CIRCULAR No. 222

UNIVERSITY OF THE WITWATERSRAND
JOHANNESBURG

PRELIMINARY CHEMICAL ANALYSES AND RAMAN SPECTROSCOPY ON SELECTED SAMPLES OF WITWATERSRAND KEROGEN

by

P. LANDAIS[1], J. DUBESSY[1], L.J ROBB[2] and C. NOUEL[1]

(1. Centre de Recherche sur la Géologie de l'Uranium, Nancy, France.
2. Department of Geology, University of the Witwatersrand, Johannesburg, Republic of South Africa.)

ECONOMIC GEOLOGY RESEARCH UNIT
INFORMATION CIRCULAR No. 222

July, 1990

PRELIMINARY CHEMICAL ANALYSES AND RAMAN SPECTROSCOPY ON SELECTED SAMPLES OF WITWATERSRAND KEROGEN

ABSTRACT

A representative suite of kerogen (or hydrocarbon) samples have been collected from a number of mines in the Witwatersrand Basin and subjected to a variety of analytical techniques including Rock-Eval pyrolysis, Raman spectroscopy and ^{13}C NMR spectroscopy. These techniques provide information on the maturity, and degree of alteration, aromatization and ordering of the hydrocarbon material which, in this preliminary report, have been compared to factors such as H/C, O/C, uranium and gold contents.

Witwatersrand kerogens are mature and highly aromatic. The hydrocarbons are structurally teterogeneous and differences exist in the Raman spectroscopic character of "seam" and "fly-speck" kerogen. An increase in the organizational degree of the hydrocarbon network is apparent as a function of increasing uranium content of the kerogen and, on a micro-scale, proximity to individual uraninite grains within the kerogen. This confirms earlier notions that hydrocarbon fixation occurred by process of radiolytic polymerization. At least two periods of hydrocarbon fixation have been observed petrographically.

oOo

PRELIMINARY CHEMICAL ANALYSES AND RAMAN SPECTROSCOPY ON SELECTED SAMPLES OF WITWATERSRAND KEROGEN

CONTENTS

Published by the Economic Geology Research Unit
Department of Geology
University of the Witwatersrand
1 Jan Smuts Avenue
Johannesburg 2001
South Africa

ISBN 1 86814 186 1

PRELIMINARY CHEMICAL ANALYSES AND RAMAN SPECTROSCOPY ON SELECTED SAMPLES OF WITWATERSRAND KEROGEN

INTRODUCTION

The abundance of solid hydrocarbon material, or kerogen, in association with many of the conglomerates of the Witwatersrand Basin is one of the more intriguing and controversial aspects concerning the formation of the gold and uranium deposits in this sequence. Several, often contradictory, points of view have been expressed in the past concerning the origin and significance of this kerogen. Early workers referred to the solid hydrocarbons as "thucholite" and viewed it as an authigenic mineral comprising an assemblage of Th, U, C, H and O (Ellsworth, 1928; Liebenberg, 1955). Detailed petrographic studies subsequently convinced Snyman (1965) that the thucholite was biogenic in origin and contained possible algal and/or fungal structures similar to sapropelic coals. This theme was developed by Hallbauer (1975) who used scanning electron microscopy to recognize the detailed structure of allegedly fossilized algae, fungi and lichen. These advanced plant forms were considered highly relevant to mineralization processes as they were believed to have trapped particulate gold and uraninite during deposition of the sediments themselves.

The plant origin of Witwatersrand kerogen has been criticized on several counts by Schidlowski (1981) who pointed to (i) the unlikelihood that eukaryotic organisms existed in the Archaean, (ii) the fact that compaction and diagenetic/metamorphic alteration would have reduced a centimetre thick lichen/fungal carpet to an extremely thin carbon seam and, additionally, destroyed delicate filamentous structures, and (iii) that the carbon content of the kerogen is inconsistent with derivation from a lichen- or fungal-like symbiont. In spite of these objections it is clear from carbon-isotope studies (Hoefs and Schidlowski, 1967) that the kerogen has a biogenic origin possibly derived from prokaryotic bacterial life-forms. Consequently, and with detailed reference to textural relationships, Schidlowski (1981) suggested that mobile hydrocarbon-bearing fluids permeated through the conglomeratic sediments and were radiolitically polymerized in areas of intense alpha-radiation represented by accumulations of pre-existing uraninite. This concept is supported by Zumberge *et al.* (1978) who pointed out that the aromaticity of Witwatersrand kerogen, as well as the high concentration of free radicals, were directly relatable to the uranium content of the kerogen and that polymerization and aromatization were, therefore, caused by nuclear irradiation. Evidence for the late remobilization of Witwatersrand kerogen is also provided by U-Pb isotope studies which have shown that carbonaceous material defines a variation curve on a concordia diagram with an upper intercept "age" of circa 2300 Ma (Allsopp *et al.*, 1986).

In recent years considerable advances have been made in the study of solid hydrocarbons associated, notably, with uranium ore-deposits. In particular, techniques such as solid-state 13-C nuclear magnetic resonance and laser-induced Raman microspectroscopy have been applied to organic matter associated with uranium deposits, with consequent improvement in the understanding of the nature, maturation and alteration of kerogens and their role in the concentration of uranium ores (Landais and Dereppe, 1985; Landais *et al.* 1990). The purpose of this report is to present preliminary chemical and Raman microspectroscopic data from a variety of Witwatersrand

kerogens and assess their relationship to parameters such as H/C and O/C ratios and uranium contents. This study is ongoing and intends utilizing a number of other analytical and interpretational techniques in the evaluation of the Witwatersrand kerogens.

SAMPLE DISTRIBUTION

A total of 28 samples from different mines representing both lateral and vertical distribution of kerogen in the Witwatersrand Basin were collected. The results of 15 of these samples are reported in the present study, with emphasis placed on kerogens from the White Reef at Randfontein, the Vaal Reef in the Klerksdorp area, the Carbon Leader in the Carletonville area and the Basal Reef, the "B" Reef, the Leader Reef and the Beisa Reef from the Welkom area. In addition, a single sample of a hydrocarbon nodule from a hydrothermally altered granite in the source area to the Witwatersrand Basin was also studied for comparative purposes.

PETROGRAPHIC CHARACTERISTICS OF WITWATERSRAND KEROGEN

Polished thin sections were cut from all the samples collected in order to study the relationships between kerogen and the enclosing conglomeratic host rocks. Detailed petrographic observations are, however, outside the scope of the present report and emphasis will be placed on only a few observations pertinent to this study.

There are two principal modes of occurrence of kerogen in the Witwatersrand conglomerates, namely "seams" which are volumetrically predominant, and "nodules" which, although common, are volumetrically less significant. Kerogen seams generally occur at the base of conglomeratic horizons, but may also anastomose and cut up through the pebble layer. The seams vary from millimetre to centimetre-scale thickness and may be massive or fibrous in texture. The latter characteristic is possibly stress imposed and analogous to vein minerals growing at right angles to the vein wall (Schidlowski, 1981). Nodular, or "fly-speck" carbon occurs as discrete, rounded-to-bulbous aggregates of solid hydrocarbon which is distributed among allogenic components within the conglomerate matrix and, for which, a satisfactory explanation has yet to be provided. Paragenetically, there is consensus (Schidlowski, 1981) that the hydrocarbons replace pre-existing uraninite, while the rich accumulations of gold commonly found in association with kerogen seams are authigenic and have been re-deposited adjacent to, or within cracks, in the kerogen.

In the context of the present study, the paragenetically late character of Witwatersrand kerogens is evident in several different forms. In Figure 1a a round uraninite grain has been fragmented and partially replaced by kerogen. A bright halo of enhanced reflection pleochroism is observed around the uraninite. An advanced state of replacement is evident in Figure 1b, where three remnant fragments, of what was conceivably a single uraninite grain, are all that remain after almost total replacement by kerogen. In Figure 1c a veinlet of kerogen, which anastomoses through a conglomerate layer, is seen to cut late hydrothermal veins of pyrrhotite. In this sample the paragenetic sequence observed is one of sulphide remobilization and pyrrhotite veining followed by mobilization of hydrocarbons and subsequent polymerization/aromatization. In Figure 1d the first recorded evidence for two distinct events of hydrocarbon mobilization

is presented. An earlier seam-like kerogen (k1) which is intimately associated with, and replaces, pre-existing uraninite, is itself cut by a later generation of uranium-deficient kerogen (k2) (Drennan, 1988).

Hydrocarbon nodules in association with uraninite are frequently observed, particularly in peraluminous granitoids in the Witwatersrand Basin hinterland. In Figure 1e a large kerogen nodule is seen intimately associated with pyrite and chalcopyrite. Closer examination of the encircled area (Figure 1f) reveals an association between uraninite and chalcopyrite, with kerogen replacing the uraninite. In other samples of peraluminous granite, uraninite occurs as discrete grains not associated with sulphides, but nevertheless generally exhibiting partial-to-extensive replacement by hydrocarbons. The paragenetic sequence between uraninite and hydrocarbons is similar, therefore, in both the hinterland granitoids and the adjacent sediments.

ANALYTICAL TECHNIQUES

Pure organic matter representative of massive kerogen seams was hand-picked after crushing of the conglomerates. No chemical treatment has been applied in order to avoid oxidation or fractionation phenomena. The purity of the organic material was checked under a binocular microscope. Several different analytical techniques were utilized during the present study of the Witwatersrand kerogen.

Elemental Analysis: Standard pyrolysis techniques (Monthioux *et al.*, 1985) provide the composition of the organic material in terms of carbon, hydrogen, oxygen and percentage ash (Table 2). Atomic H/C and O/C ratios are calculated from these data and plotted on a Van Krevelen diagram. Analyses of Au, U, Fe, Pb, Zn, Cu were also performed by atomic absorption techniques (Table 1).

Rock-Eval Pyrolysis: This is an open-medium pyrolysis technique (Monin *et al.*, 1980) which determines the hydrocarbon potential, and the parameter Tmax which is an indication of maturity or aromatization. Samples were heated in a medium swept by an inert gas at 550°C and syphoned at a constant rate. Free hydrocarbons released up to 250°C were trapped and analyzed by Flame Ionization Detector (FID) as a first-peak S1. Hydrocarbons generated between 250 and 550°C are derived from the cracking of the kerogen and are analyzed by FID as a second peak S2. The area of the S2 peak is ratioed to the carbon content providing the Hydrogen Index (HI). The maximum hydrocarbon generation temperature (top of the S2 peak) is called Tmax (°C). CO_2 produced during the pyrolysis is recorded as a third peak S3, which is also ratioed to the carbon content to give the Oxygen Index (OI) (Table 2).

Raman Microspectroscopy: This is a spectroscopic technique which provides information on the degree of organization of the hydrocarbon network. Two peaks are recorded: the first one at around 1610 cm^{-1} which corresponds to the C-C vibrations and the second peak around 1340 cm^{-1} which represents the defects in the organic skeleton. Data are recorded as the heights of the two peaks and presented in Table 3 as peak height ratios. The inter-peak height at 1500 cm^{-1} is also recorded. The half height width (1/2 H 1610) of the 1610 peak is also calculated as an inverse measure of the aromaticity. The peak ratio 1610/1340 represents a good approximation of the organization of the kerogen structure. Micro-Raman analyses were

performed on a multichannel X-Y Dilor spectrometer. The excitation radiation is the 514.5 nm line of an Ar laser set at a low power (below 5mw) in order to minimise alteration of organic matter. An Olympus microscope fitted with X50 and X100 objectives is used to locate the beam on the sample point. Integration time of 20 seconds for 5 and 10 accumulations were considered adequate for recording of spectra. Spectral bands were integrated and emphasis placed on the E2g2 band attributed to C-C vibrations of aromatic carbons (located at 1575 cm^{-1} for perfect graphite) and the "1350 cm^{-1}" band which is assigned as a defect band (Tuinstra and Koenig, 1971). Peak wave numbers of the two bands were recorded.

^{13}C NMR Spectroscopy: Solid state ^{13}C Nuclear Magnetic Resonance spectroscopy is a very promising technique for analyzing solid insoluble organic material. Present data have been obtained on a Brucker CXP 100 spectrometer at the Lourain University (Belgium). Measurements were made according to the technique previously described in Dereppe *et al.* (1983). NMR spectra have been divided into bands corresponding to oxygen-bearing, aromatic and saturated carbons (Landais *et al.*, 1988). Absolute quantitative aspects of NMR data are still debated in literature (Hagaman *et al.*, 1986) and consequently data will be mostly discussed from a comparative view. Parameters such as the aromaticity factor (Fa= percentage of total organic carbon), degree of substitution of aromatic rings and methyl/methylene ratio will be referred to in the discussion, but the data will be presented at a later stage.

INTERPRETATION OF DATA

When elemental composition is plotted on a Van Krevelen diagram (Figure 2), it is apparent from the range of H/C ratios (i.e. between 0.55 and 0.40) that Witwatersrand kerogens are highly mature, plotting at the end of the catagenetic zone, i.e. the gas-producing zone. However, Witwatersrand samples plot in a part of the Van Krevelen diagram which does not entirely correspond with the accepted composition of algal-derived kerogens. This feature is consistent with the Tmax values which range between 440 and 490°C (Figure 3) and indicate mature to over-mature compositions. Similarly, hydrocarbon potential (HI) is low and ranges between 20 and 100 mg hydrocarbon /g of total organic carbon (Figure 3).

The NMR aromaticity factor ranges between 63% and 90% (with the exception of 1 sample) and increases with decreasing hydrocarbon potential (Figure 4). Furthermore, the degree of aromatic substitution exhibits a very good correlation with the methyl/methylene ratio (Figure 5). This indicates that substitution of the hydrocarbon is achieved by very short aliphatic chains.

Oxidation

The trends recorded in Figures 2 and 3 cannot be interpreted as a maturation series and the trend of decreasing H/C with increasing O/C generally corresponds to an oxidation phenomenon. Similarly, the HI versus Tmax trend (Figure 3) is also typical of an oxidation process. It must be noted that the correlation factors derived from regression lines are in both cases above 0.5 and suggest that all the samples have been involved to

differing degrees in the same alteration process. This oxidation process may be related to either of two processes, namely, leaching of the kerogen by oxidizing hydrothermal fluids or involvement of kerogen in oxidation-reduction processes during ore remobilization (see later). The trend observed in Figure 2 has already been noted in other sedimentary uranium deposits and has been interpreted as a late diagenetic phenomenon. Finally, it is pertinent to note that the Witwatersrand kerogen exhibits a restricted degree of oxidation and cannot, therefore, be related to atmospheric processes.

Organization of Kerogen Structure

Raman spectral data plotted in Figures 6, 7 and 8 provide indications regarding the structural ordering of the Witwatersrand kerogens. The results indicate that the 1340-1350 cm^{-1} peak (which is absent in graphitic material) is as well-developed as the 1600 cm^{-1} peak indicating the presence of defects in the carbon structure and pointing to the fact that the Witwatersrand kerogen is poorly organized structurally. Similar spectra have been recorded in bitumens from the unconformity-related Saskatchewan uranium deposits of Saskatchewan.

Results from micro-Raman spectra recorded in portions of carbon seams distinctly removed from (i.e. more than 100µm) individual uraninite grains are plotted in Figure 7 which displays the intensity ratio of the two main bands versus the half height width of the 1600cm^{-1} band. Contrary to the meta-anthracite or graphite series, which generally exhibit a good correlation between the 1600cm^{-1} band width and the 1600/1350 intensity ratio (Oh, 1987; Wang *et al.*, 1989), no significant relationship is observed in the Witwatersrand samples. The scattering of the carbon seam samples (full squares) along the X-axis can be roughly correlated with the uranium content of the organic matter (i.e. a broadening of the 1600 cm^{-1} band is observed with increasing uranium content). Such variations could be explained by hydrocarbon fixation due to radiolytic polymerization by beta- and gamma-radiation. On the other hand, micro-Raman spectra recorded within the large, highly pleochroic, halos surrounding individual uraninite grains, display a sharper 1600cm^{-1} band than that for spectra recorded outside the halo. This suggests an increase in the degree of organization of the carbon network in the halo area which is consistent, either with a thermal effect (Oh, 1987), or possibly alpha-radiation immediately adjacent to the uraninite grain. The diameter of the pleochroic halo is similar to the length of the alpha-particle path (40-50 µm) and it is this feature that could account for the observed variations in the Raman spectral characteristics.

Late uranium-deficient hydrocarbon seams which cross-cut earlier seams have been observed in thin section (Figure 1d) and also analysed by micro-Raman spectroscopy. The late kerogen is clearly differentiated in Figure 7 (star) where it is characterized by a significantly higher 1600/1350 intensity ratio. This late kerogen vein is not associated with uraninite.

The general spectral characteristics of fly-speck carbon shown in Figure 7 are broadly similar to those of the carbon seams. However, when both types of kerogen are present in the same thin section (see boxed sample points in Figure 7), the 1600 cm^{-1} peak half height width of the fly-speck carbon is higher. Furthermore, half height width of the 1350 cm^{-1} peak in fly-speck carbon spectra range between 140 and 165 cm^{-1}

whereas the range is between 115 and 130 cm^{-1} in carbon seams. This suggests that the structure of the fly-speck carbon is less organized than that of carbon seams, implying a lower degree of radiolytic polymerization.

Micro-Raman investigations also clearly distinguish between the fly-speck kerogen in the reefs and kerogen nodules obtained from granites in the Witwatersrand source area (Figure 8). The latter generally exhibit higher 1600/1350 ratios and higher half height widths of the 1600 cm^{-1} peak.

Relation to Uranium and Gold Contents

U and Au contents of the kerogen samples have been determined and reported in Table 1. Significant ranges in both elements are observed in the samples. U content is well correlated to a variety of different organic parameters. As an example Figure 9 reveals an inverse correlation between U% and H/C. Similarly, Figure 10 which plots uranium content versus NMR methyl/methylene ratio reveals a good correlation between these two parameters. Such relationships can be interpreted as indicating a loss of hydrogen and progressive removal of aliphatic chains in the kerogen during either reduction or radiolytic degradation. As far as the present results are concerned, it remains impossible to determine what process is responsible for such a correlation, although the trend is consistent with the observations that hydrocarbons replace uraninite and hence their structure and composition are likely to be related to the intensity of nuclear irradiation (or uranium concentration). Further micro-Raman and micro infra-red analyses will be devoted to analyze in more detail the influence of radiolytic alteration around uraninite grains.

No important correlation has been found between gold content and organic parameters, with the exception of the O/C vs Au% plot (Figure 11) where all but one of the samples reveal a negative correlation. It appears here that the more reduced the kerogen, the higher the gold content. Finally, it is pertinent to note that on the scale of the kerogen samples studied here, there is no simple correlation between gold and uranium contents (Figure 12). These observations are consistent with the sequential paragenetic characteristics outlined above. Although the organizational characteristics of the kerogen are clearly related to the abundance of uraninite and the proximity to individual uraninite grains, there is no such relationship that exists with respect to the gold content of the kerogen. Gold has, however, been precipitated in and around kerogen as a result of fluid-hydrocarbon interaction and it is, therefore, possible that gold contents will be correlatable in some way to kerogen composition (e.g. Figure 12). However, because the gold and uraninite associated with kerogen are unrelated in terms of paragenesis and mineralization process there is no expectation of Au-U correlation on a small scale.

CONCLUSIONS

These preliminary results described above allow the following conclusions to be made at this stage:-

(i) The organic material from the Witwatersrand Basin exhibits a highly aromatic structure which corresponds with mature to over-mature kerogens.

(ii) The organic material is heterogeneous in terms of chemical structure. Within the same seam, petrographic studies have confirmed the existence of at least two generations of kerogen, while micro-

Raman spectra indicate variations in the chemical structure as a function of proximity to uraninite grains and uranium content. It is apparent that radiolytic processes provoke localized variations that can only be detected through micro-analytical techniques.

(iii) Variations in the chemical structure are observed between hydrocarbons analysed in seams, "fly-specks" and nodules within hydrothermally altered granites.

(iv) Whereas variations in chemical composition and organizational structure of kerogen can be related to the uranium content, the correlation between these parameters and gold content is less obvious.

Further studies are needed in order to confirm and elaborate upon the conclusions presented above. Additional work will deal, especially, with:-

1. Micro-scale characterization of the kerogens with emphasis on the effects of radiolysis. Further micro infra-red and Raman spectroscopy will be carried out.
2. Global analyses of carbon seams in order to obtain the precise chemical structure of the kerogen. Complementary NMR analyses, as well as additional pyrolysis, gas chromatography and mass spectrometry investigations are currently underway.

ACKNOWLEDGEMENTS

This research was supported by global operating and visitors grants from the CSIR-FRD to LJR and PL respectively. Grateful thanks go to the numerous geological and mining personnel from the following mines, who generously assisted in the collection of organic material:- Doornfontein, Deelkraal, Hartbeesfontein, Free Gold, Consolidated Modderfontein, Randfontein Estates, Loraine, Vaal Reefs and Kinross.

REFERENCES

Allsopp, H.L., Evans I.B., Giusti, L. Hallbauer, D.K., Jones, M.Q.W., and Welke, H.J. (1986). U-Pb dating and isotopic characterization of carbonaceous components of the Witwatersrand reefs. Ext. Abstr., Geocongress '86, Johannesburg, 85-88.

Dereppe, J.M., Boudon, JO., Moreaux, C., and Durand, B. (1983). Structural evolution of a sedimentologically homogeneous coal series as a function of carbon content by solid state ^{13}C NMR. Fuel, 62, 375-389.

Drennan, G.R. (1988). The nature of the Archaean basement in the hinterland to the Welkom Goldfield. Unpubl. M.Sc. dissertation, Univ. Witwatersrand, Johannesburg, 187pp.

Ellsworth, H.V. (1928). Thucholite - a remarkable primary carbon mineral from the vicinity of Parry Sound, Ontario. Amer. Mineral., 13, 419-441.

Hagaman, E.W., Rife Chambers, R. Jr., and Woody, M.C. (1986). Determination of the fraction of organic carbon observable in coal and coal derivates measured by high resolution solid-state ^{13}C nuclear magnetic resonance spectrometry. Anal. Chem., 58, 387-394.

Hallbauer, D.K. (1975). The plant origin of the Witwatersrand carbon. Mineral Sci. Eng., 7, 111-131.

Hoefs, J., and Schidlowski, M. (1967). Carbon isotope composition of carbonaceous matter from the Precambrian of the Witwatersrand System. Science, 155, 11096-1097.

Landais, P. and Dereppe, J.M. (1985). A chemical study of the carbonaceous material from the Carswell Structure. *In:* Laine, R. et al. (Eds.). The Carswell Structure Uranium Deposits. Geol. Assoc. Canada Spec. Paper 29, 165-174.

Landais, P., Monthioux, M., Dereppe, J.M., and Moreaux, C. (1988). Analyses of insoluble residues of altered organic matter by ^{13}C CP/MAS nuclear magnetic resonance. Org. Geochem., 13, 1061-1066.

Landais, P., Dubessy, J., Meyer, A.J., and Robb, L.J. (1990). The importance of organic geochemistry in the understanding of uranium ore-forming processes. Org. Geochem., in press.

Liebenberg, W.R. (1955). The occurrence and origin of gold and radioactive minerals in the Witwatersrand System, the Dominion Reef, the Ventersdorp Contact Reef and the Black Reef. Trans. geol. Soc. S. Afr., 58, 101-254.

Monin, J.C., Durand, B., Vandenbroucke, M., and Huc, A.Y. (1980). Experimental simulation of the natural transformation of kerogen. *In:* Douglas A.G. and Mawell J.R. (Eds.). Advances in Organic Geochemistry 1979, 517-530.

Monthioux, M., Landais, P., and Monin, J.C. (1985). Comparison between natural and artificial maturation series of humic coals from the Mahakam Delta, Indonesia. Org. Geochem., 8 (4), 275-292.

Oh, J.O. (1987). Etude structurale de la graphitation naturelle (exemple des bassins Sud-Coréens). Ph.D. Thesis, Univ. Orleans, France, 181pp.

Schidlowski, M. (1981). Uraniferous constituents of the Witwatersrand conglomerates: ore-microscopic observations and implications for Witwatersrand metallogeny. *In:* Armstrong, F. (Ed.). Genesis of Uranium- and Gold-bearing Precambrian Quartz-pebble Conglomerates. U.S. Geol. Surv. Prof. Pap., 1161, 1-29.

Snyman, C.P. (1965). Possible biogenetic structures in Witwatersrand thucholite. Trans. geol. Soc. S. Afr., 68, 225-233.

Tuinstra, F. and Koenig, J.L. (1970). Raman spectrum of graphite. J. Chem. Phys, 53, 1726-1130.

Wang, A., Dhamelincourt, P., Dubessy, J., Guerard, D., Landais, P., and Lelaurain, M. (1989). Characterization of graphite alteration in a uranium deposit by micro-Raman spectroscopy, X-ray diffraction, transmission electron microscopy and scanning electron microscopy. Carbon, in press.

Zumberge, J.E., Sigleo, A.C., and Nagy, B. (1978). Molecular and elemental analyses of the carbonaceous matter in the gold and uranium bearing Vaal Reef carbon seams, Witwatersrand Sequence. Mineral. Sci. Eng. 10, 223-246.

oOo

T A B L E 1

CHEMICAL CHARACTERISTICS OF WITWATERSRAND KEROGEN

	SAMPLES	U %	Au %	Fe %	Pb %	Zn ppm	Cu ppm
1	VAAL REEF	7,5	1,8	3,5	2,2	175	250
2	VR 1	10,4	0,73	2,4	2,7	1700	630
3	VR 1a	8,8	0,31	4,0	2,2	82	250
4	VR 2	11,5	0,0085	2,0	4,7	10500	490
5	DN D1	2,0	0,42	0,4	0,3	32	250
6	DN 3531	2,2	0,27	1,4	0,5	32	880
7	HB 3	7,7	1,47	5,0	2,3	107	270
8	HB 4	5,3	1,1	5,2	1,6	100	310
9	FSG B.R.	4,0	0,46	0,23	1,4	62	100
10	BP 7735	8,5	-	-	-	-	-
11	BP 7743	3,1	-	-	-	-	-
12	COOK	8,2	4,7	6,6	10,2	12000	950
13	LOR 3	7,1	0,67	7,6	2,4	150	320
14	LEADER	8,8	0,0300	3,0	3,5	375	80
15	WHITE	5,8	0,0260	2,3	1,8	325	80

TABLE 2

ORGANIC CHARACTERISTICS OF WITWATERSRAND KEROGEN

	SAMPLES	H/C at	O/C at	C %	T max	PC %	HI(mg/gT C)	OI(mg/gT C)	S1(mg/gT C
1	VAAL REEF	0,499	0,051	54,1	466	24	51	4	3,5
2	VR 1	0,464	0,074	53,0	474	20	36	6	3,1
3	VR 1a	0,423	0,070	52,0	476	22	42	4	2,4
4	VR 2	0,423	0,074	52,2	465	12	26	5	0,9
5	DN D1	0,488	0,065	75,2	464	33	53	9	2,6
6	DN 3531	0,550	0,030	80,8	458	62	87	4	2,5
7	HB 3	0,491	0,054	43,5	475	17	36	3	3,2
8	HB 4	0,525	0,054	50,6	457	23	50	5	4,3
9	FSG B.R.	0,462	0,067	77,8	469	28	43	8	1,1
10	BP 7735	0,490	0,054	59,3	476	-	36	7	2,1
11	BP 7743	0,550	0,057	78,7	459	-	55	6	1,0
12	COOK	-	-	36,6	456	8	21	16	2,2
13	LDR 3	-	-	27,8	447	18	92	7	3,4
14	LEADER	-	-	40,2	444	13	35	16	3,8
15	WHITE	-	-	55,2	490	9	15	18	2,8

Tmax - Temperature of maximum hydrocarbon generation

PC% - Pyrolizable carbon (% released during pyrolysis)

HI - Hydrogen Index (i.e. ratio of S2 pyrolysis peak to total organic carbon)

OI - Oxygen Index

S1 - Free hydrocarbon peak (S1 pyrolysis peak)

TABLE 3

RAMAN SPECTROMETRIC CHARACTERISTICS OF WITWATERSRAND KEROGEN

	SAMPLES	1610/1500	1500/1340	1610/1340	1/2H 1610
1	TKB 3(120C)	3,00	0,43	1,30	95,0
2	3531/DN	4,29	0,26	1,10	67,5
3	HB 2	4,27	0,26	1,12	65,0
4	LOR 4	3,96	0,29	1,13	70,0
5	LEADER	3,12	0,41	1,27	80,0
6	DN 3135 IE	4,38	0,28	1,22	62,5
7	FSG B.R.	3,24	0,39	1,24	67,5
8	BEISA REEF	4,29	0,26	1,12	52,5
9	VR 1	3,50	0,34	1,21	78,0
10	D1 DN	3,45	0,34	1,16	75,0

Figure 1

a. Uraninite grain partially replaced by kerogen. Note the pleochroic halo that extends for approximately 20 microns around the uraninite grain. Field of view $\simeq$ 200 microns

b. Remnants of a single fragmented grain of uraninite almost totally replaced by kerogen. Field of view $\simeq$ 200 microns.

c. Vein (or seam) of kerogen cutting through late-stage authigenic pyrrhotite veinlets. Field of view $\simeq$ 1000 microns.

d. Kerogen seam containing numerous replaced uraninite grains (K1) cut by a later veinlet of kerogen (K2) not associated with uraninite. Field of view $\simeq$ 1000 microns.

e. Veinlet of pyrite, chalcopyrite and uraninite in hydrothermally altered peraluminous granite from the hinterland to the Witwatersrand Basin. Nodule of kerogen partially replaces chalcopyrite and uraninite. Field of view $\simeq$ 1000 microns. Boxed area shown enlarged in Figure 1f.

f. Close up of previous microphotograph showing partial replacement of chalcopyrite (cpy) and uraninite (u) by kerogen (k). Field of view $\simeq$ 150 microns.

Figure 1

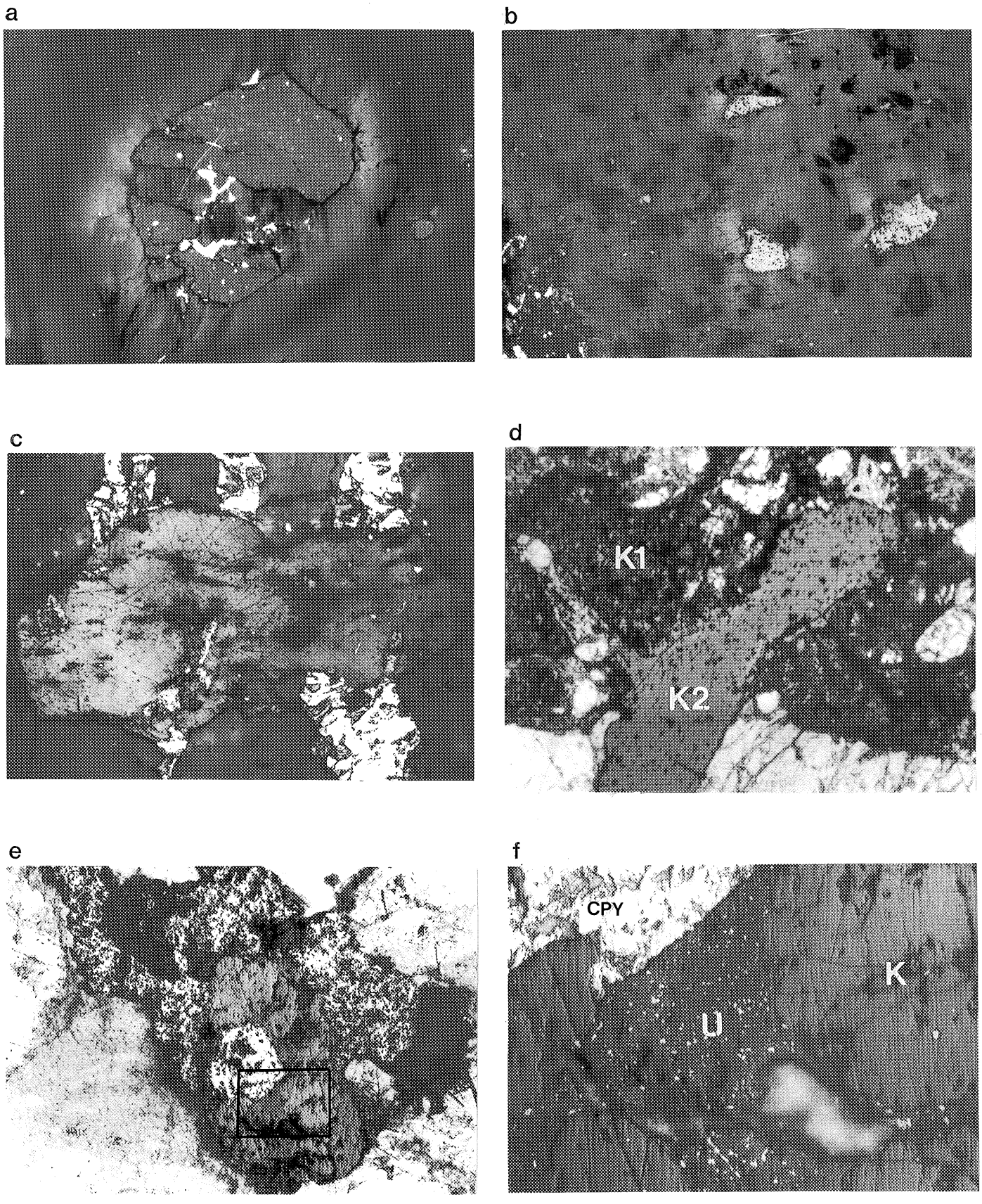

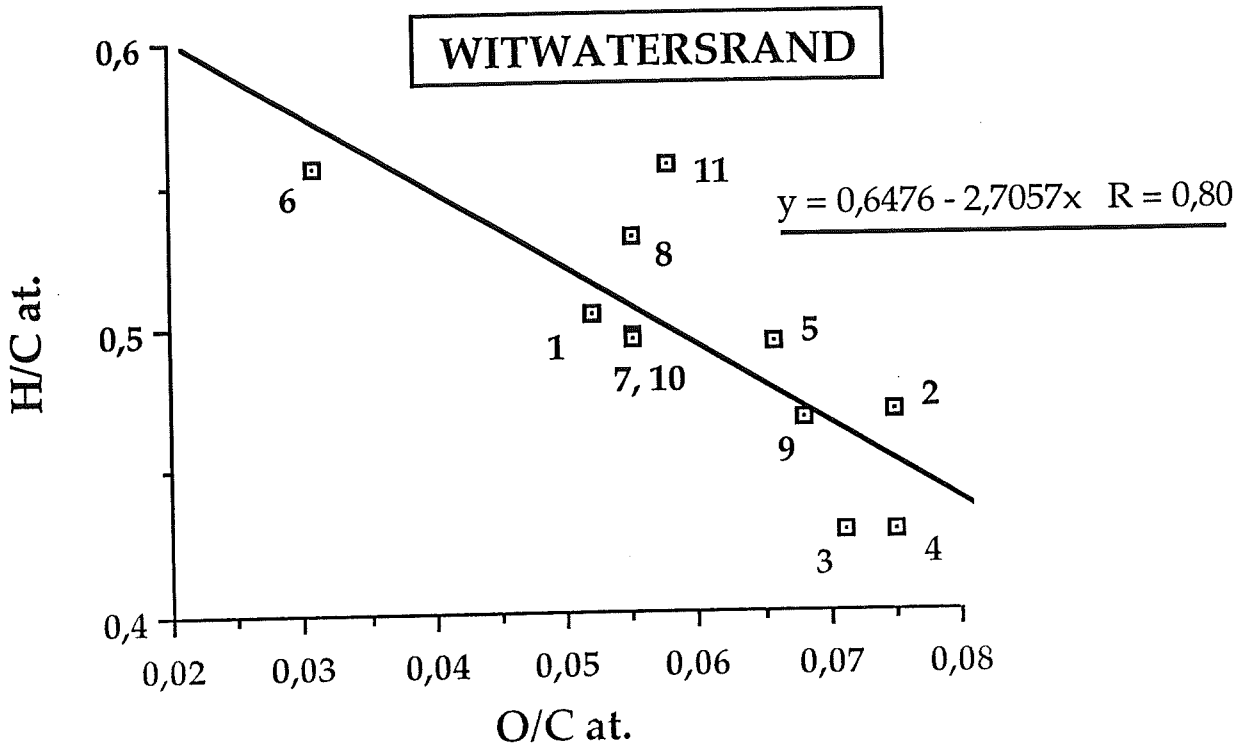

Figure 2: Van Krevelen-type diagram plotting atomic proportions of H/C versus O/C for Witwatersrand kerogen. Data from Table 2.

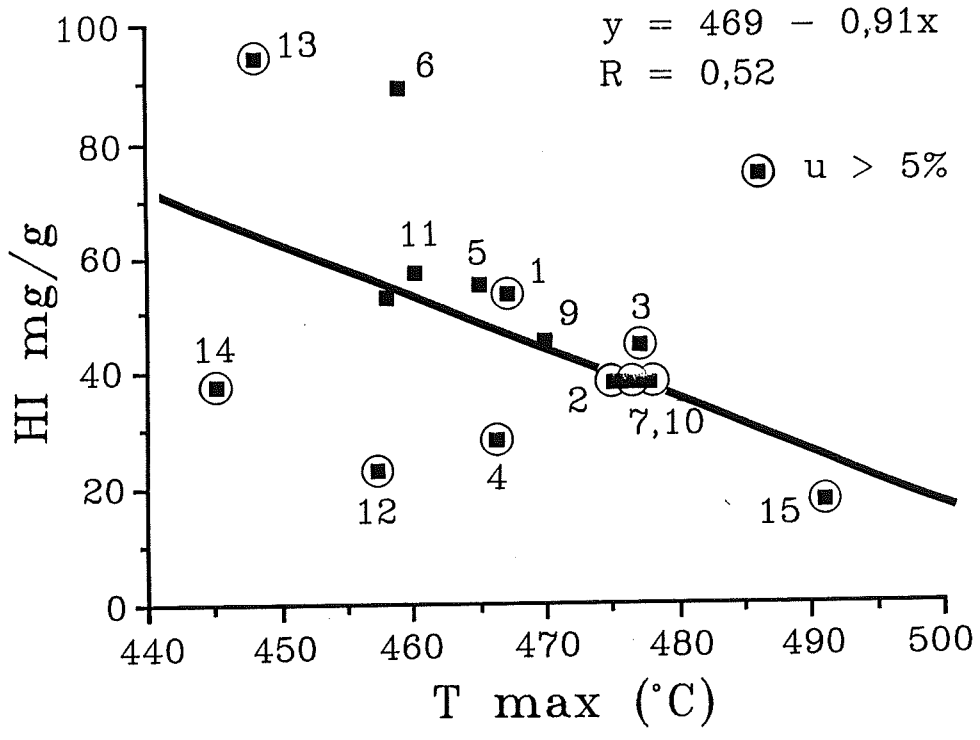

Figure 3: Plot of Hydrogen Index versus Temperature of maximum hydrocarbon generation for Witwatersrand kerogen. Data from Table 2.

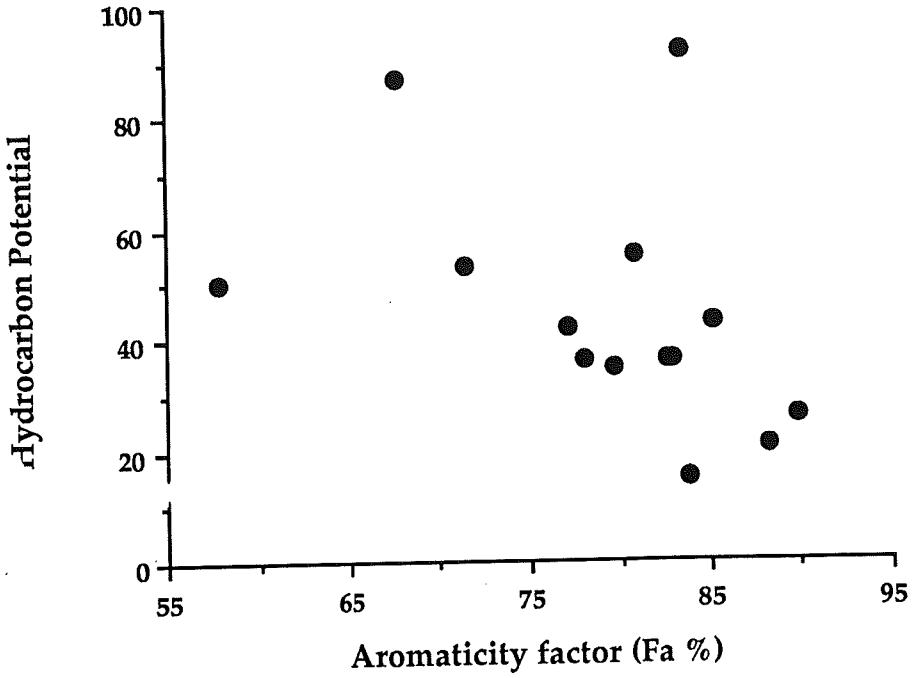

Figure 4: Plot showing the inverse relationship between Hydrocarbon Potential and Aromaticity Factor for Witwatersrand kerogen

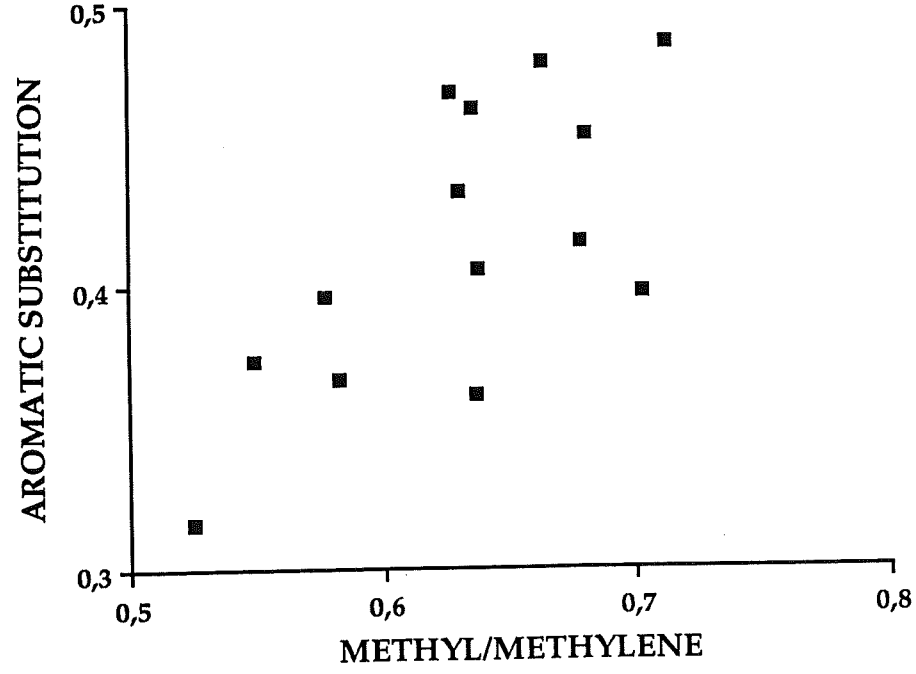

Figure 5: Plot showing the positive correlation between Aromatic Substitution and the Methyl/Methylene ratio for Witwatersrand kerogen

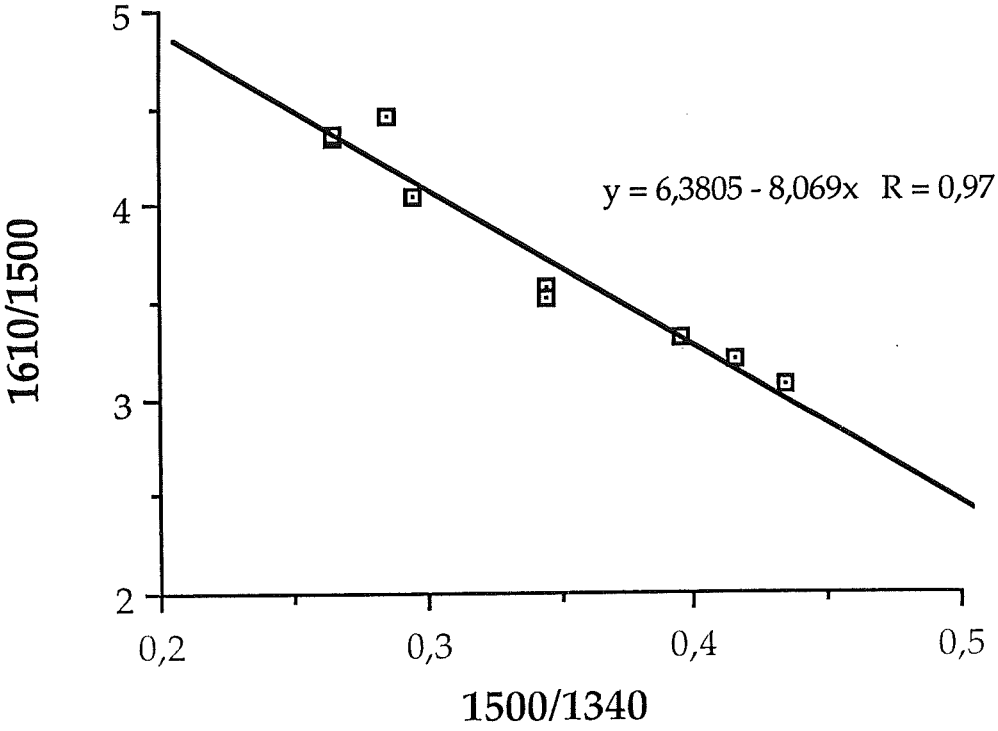

Figure 6: Plot showing the inverse relationship between the 1610/1500 peak intensity ratio and the 1500/1340 peak intensity ratio as obtained from micro-Raman spectroscopy. Data from Table 3.

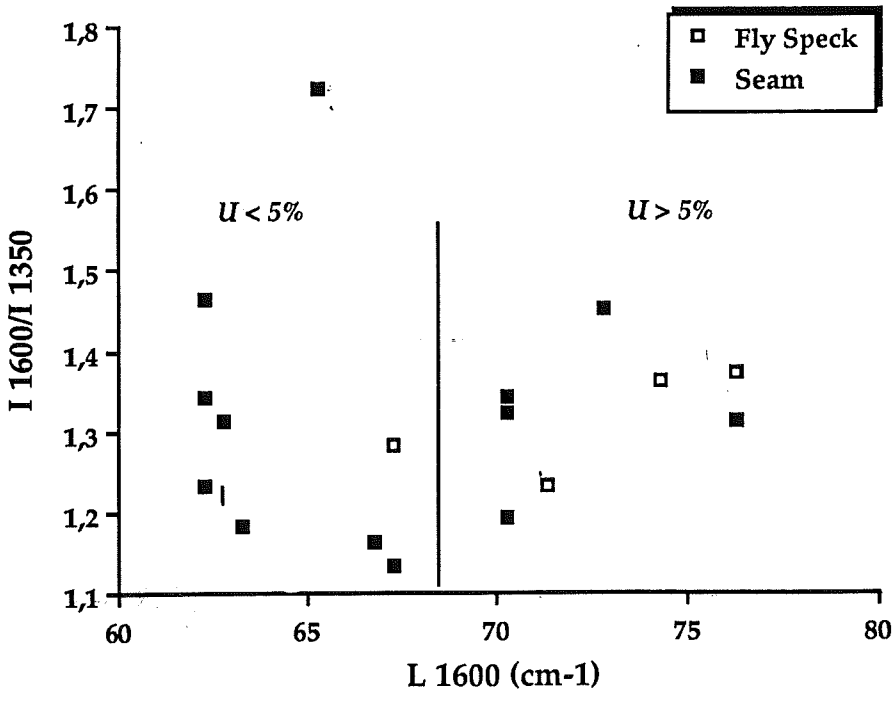

Figure 7: Plot of the 1600/1350 peak intensity ratio versus the half-height width of the 1600 cm^{-1} peak from Raman analyses for seam and "fly-speck" kerogen in the Witwatersrand reefs. The relationship of uranium content to the abscissa variable is clearly demonstrated. The two boxed sample points represent seam and "fly-speck" kerogen from the same sample. Data from Table 3.

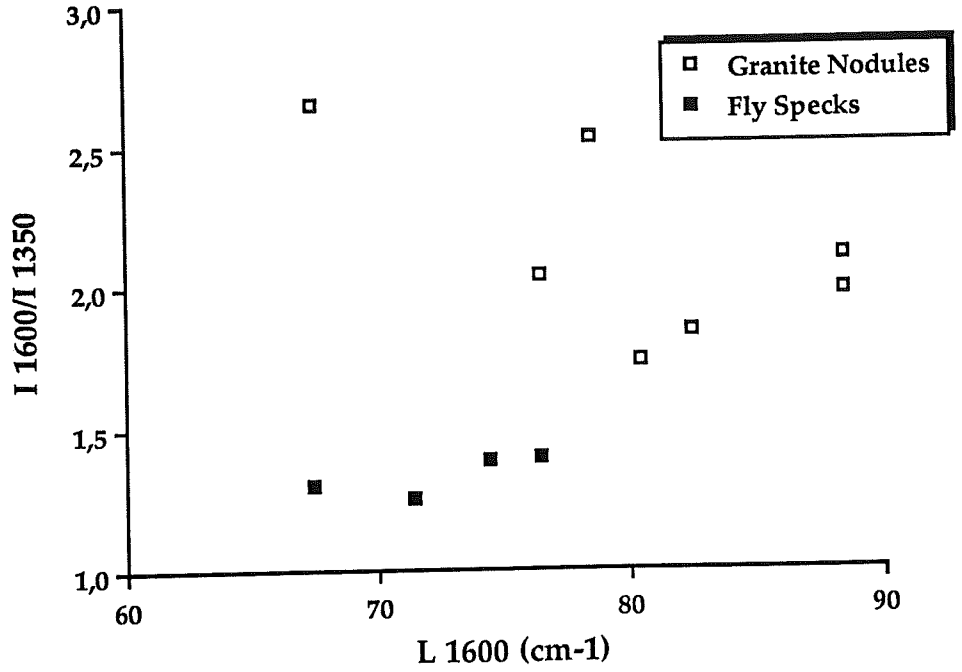

Figure 8: Plot of the 1600/1350 peak intensity ratio versus the half-height width of the 1600 cm^{-1} peak from Raman analyses comparing "fly-speck" kerogen from the Witwatersrand reefs to hydrocarbon nodules from hydrothermally altered granites in the hinterland

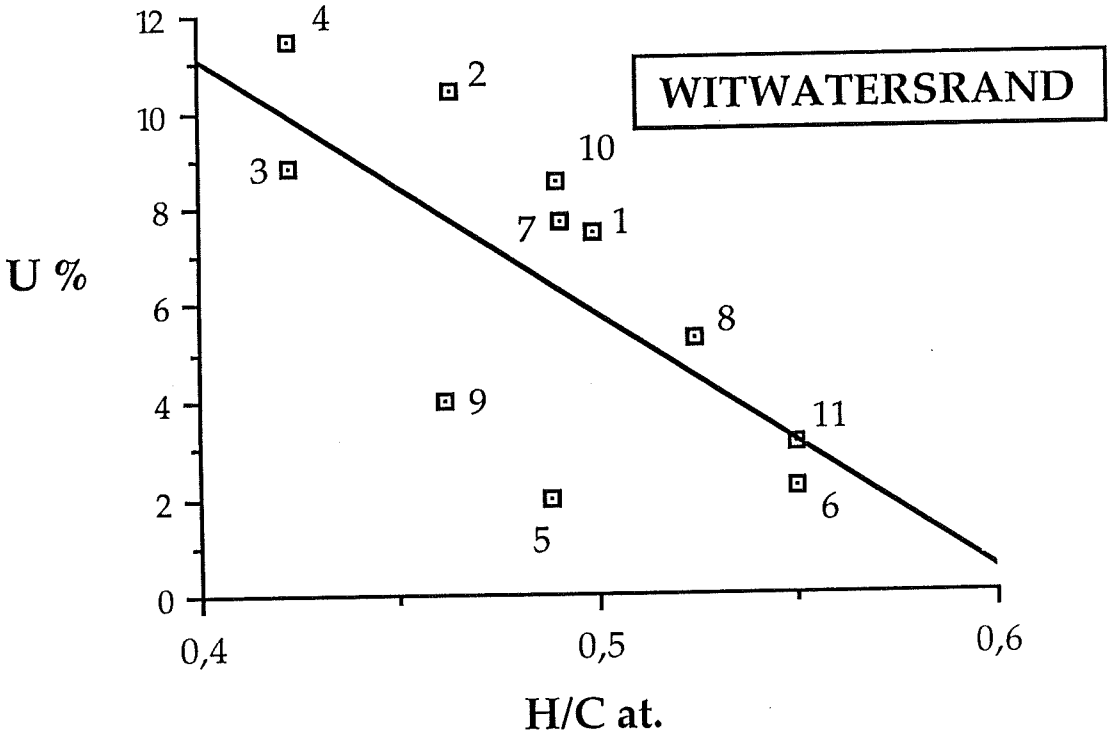

Figure 9: Plot showing the inverse correlation between the uranium content of kerogen and the H/C atomic ratio. Data from Tables 1 and 2.

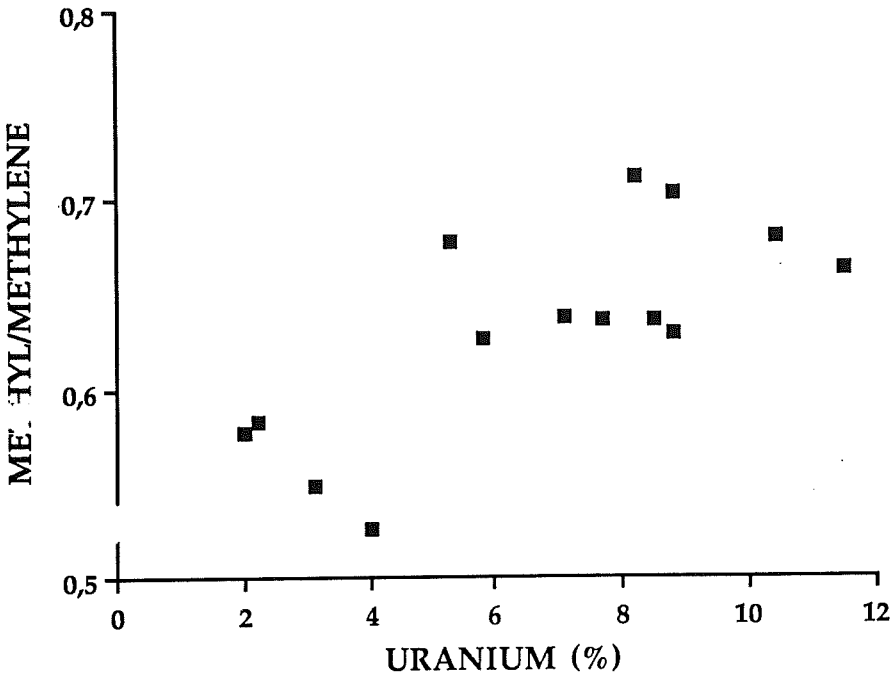

Figure 10: Plot showing the positive correlation between uranium content of kerogen and the methy/methylene ratio as derived from the NMR data

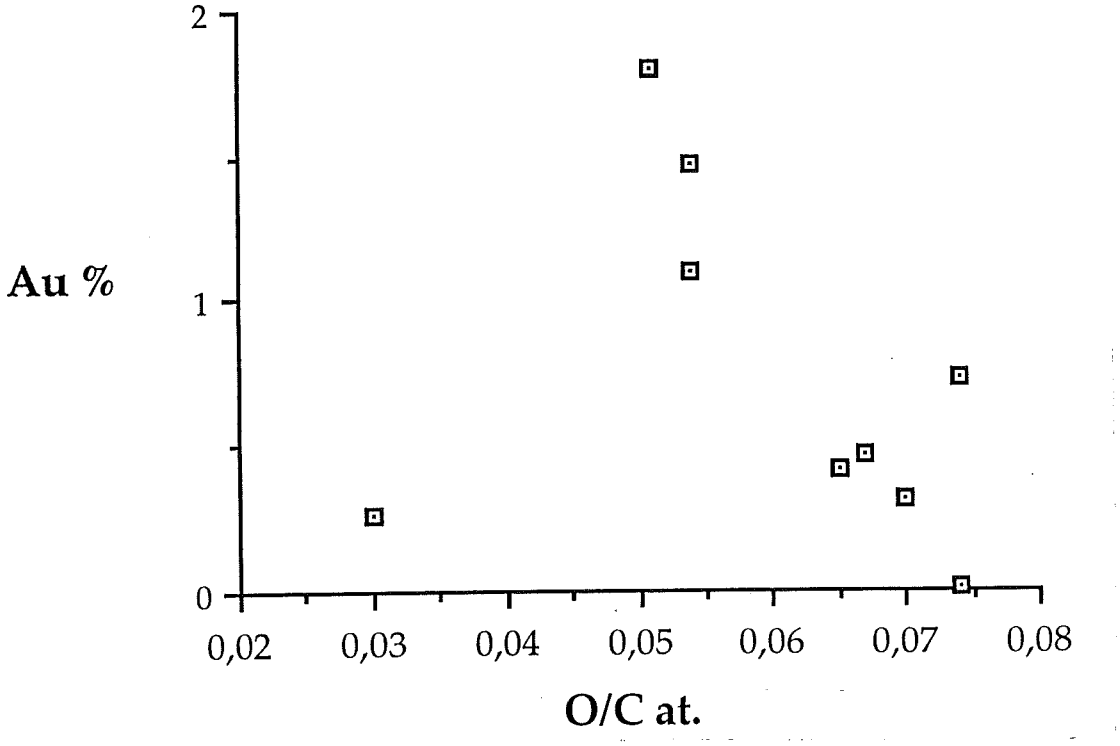

Figure 11: Plot illustrating the apparent correlation between gold content of kerogen and the O/C atomic ratio. No explanation is provided for the discrepant point. Data is from Tables 1 and 2.

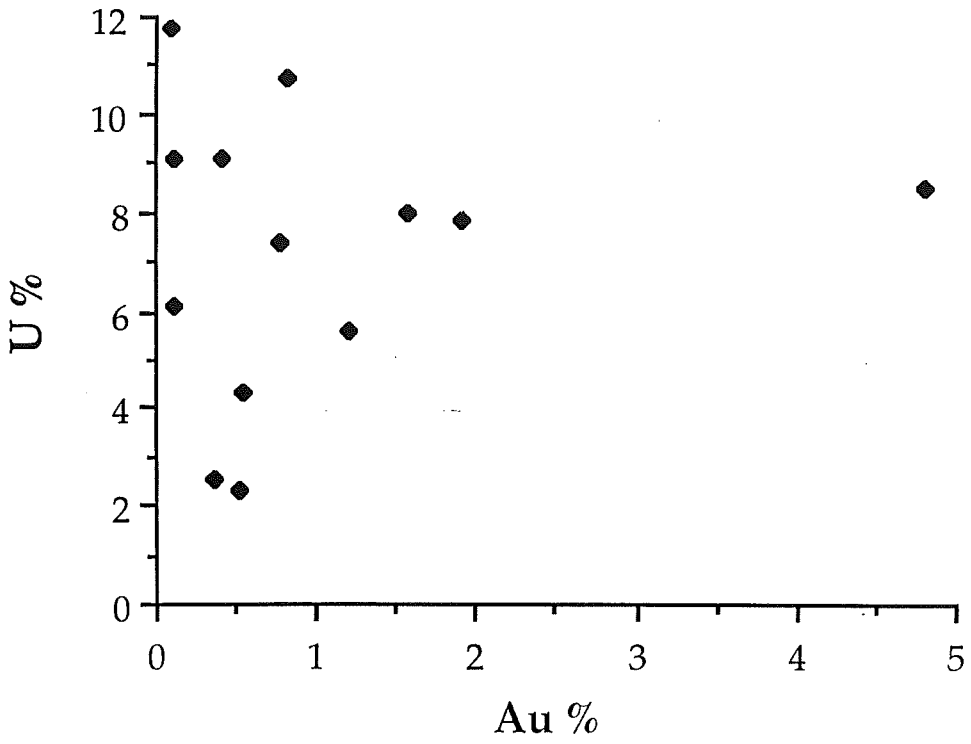

Figure 12: Plot showing the lack of correlation between the gold and uranium contents of kerogen in Witwatersrand reefs. Data is from Table 1.